Journal of Hazardous Materials 192 (2011) 1046–1055

Contents lists available at ScienceDirect

Journal of Hazardous Materials

journal homepage: www.elsevier.com/locate/jhazmat

Taguchi optimization approach for Pb(II) and Hg(II) removal from aqueous solutions using modified mesoporous carbon

Ghasem Zolfaghari [a], Abbas Esmaili-Sari [a], Mansoor Anbia [b,*], Habibollah Younesi [a], Shahram Amirmahmoodi [b], Ali Ghafari-Nazari [c]

[a] Department of Environment, Faculty of Natural Resources and Marine Sciences, Tarbiat Modares University, Noor, Mazandaran, P.O. Box: 46414-356, Iran
[b] Research Laboratory of Nanoporous Materials, Faculty of Chemistry, Iran University of Science and Technology, Farjam Street, Narmak, Tehran 16846, Iran
[c] Loabiran Company, Research and Development Group, Shiraz, Iran

ARTICLE INFO

Article history:
Received 22 January 2011
Received in revised form 2 June 2011
Accepted 6 June 2011
Available online 12 June 2011

Keywords:
Lead
Mercury
Zn-OCMK-3
Taguchi method
Adsorption

ABSTRACT

Using the Taguchi method, this study presents a systematic optimization approach for removal of lead (Pb) and mercury (Hg) by a nanostructure, zinc oxide-modified mesoporous carbon CMK-3 denoted as Zn-OCMK-3. CMK-3 was synthesized by using SBA-15 and then oxidized by nitric acid. The zinc oxide was loaded to the modified CMK-3 by the equilibrium adsorption of Zn(II) ions from aqueous solution followed by calcination to convert zinc nitrate to zinc oxide. The CMK-3 had porous structure and high specific surface area which can accommodate zinc oxide in a spreading manner, the zinc oxide connects to the carbon surface via oxygen atoms. The controllable factors such as agitation time, initial concentration, temperature, dose and pH of solution have been optimized. Under optimum conditions, the pollutant removal efficiency (PRE) was 97.25% for Pb(II) and 99% for Hg(II). The percentage contribution of each controllable factor was also determined. The initial concentration of pollutant is the most influential factor, and its value of percentage contribution is up to 31% and 43% for Pb and Hg, respectively. Our results show that the Zn-OCMK-3 is an effective nanoadsorbent for lead and mercury pollution remediation. Langmuir and Freundlich adsorption isotherms were used to model the equilibrium adsorption data for Pb(II) and Hg(II).

1. Introduction

Heavy metal contamination such as lead (Pb) and mercury (Hg) has been identified as a concern in environment, due to discharges from industrial wastes, agricultural and urban sewage [1]. Pb has been well recognized for its negative effect on the environment where it accumulates readily in living systems [2]. There is a great concern about Hg pollution, which is due to its toxicity, persistent character in the environment and biota as well as biomagnification along the food chain [3]. Increasing pollution by Pb and Hg has been reported in recent years in Iran [4,5]. The results from the data collected in the rivers around Caspian Sea and Anzali Wetland, North Iran, show the various degrees of Pb and Hg concentrations [6]. Thus, the increased awareness of toxicity of heavy metal and the stringent environmental safety regulations demand the removal of them from the various discharges to avoid contamination of the biological ecosystem. Several methods such as coagulation [7], chemical oxidation [8], photocatalytic degradation [9], adsorption [10], etc. are being used for the removal of heavy metal from water. Among these methods, adsorption is still the most versatile and widely used. Alternative adsorbents studied include biosorbents [11], clays [12], activated carbon [13], resins [14] and zeolites [15]. Increasingly stringent standard on the quality of drinking water has stimulated a growing effort on the development of new high efficient adsorbents. The development of porous materials with large surface areas is currently an area of extensive research, particularly with regard to potential applications as environmental remediation. An upsurge began in 1992 with the development by the Mobil Oil Company of the class of silicate mesoporous materials known as the M41S phase [16]. It was reported that ordered mesoporous silica (OMS) can be used as an adsorbent for removal of numerous compounds [17–19]. Recently, the synthesis of ordered mesoporous carbons (OMC) using OMS as hard templates has attracted a great deal of attention. Ryoo et al. [20] first used MCM-48 silica as the template to synthesize CMK-1 carbon. Subsequently, this research group reported the synthesis of CMK-2 [21], CMK-3 [22], CMK-4 [23], and CMK-5 [24]. Very recently, Guo et al. [25] reported the synthesis of OMC by using SBA-16. Some researchers modified and functionalized the surface of the OMC for more applications [26,27]. In the present study, CMK-3 was synthesized using SBA-15, modified by HNO_3 treatment and then functionalized by $Zn(NO_3)_2{\cdot}4H_2O$. This modified nanostructure,

* Corresponding author. Tel.: +98 21 77240516; fax: +98 21 77491204.
E-mail address: anbia@iust.ac.ir (M. Anbia).

0304-3894/$ – see front matter © 2011 Elsevier B.V. All rights reserved.
doi:10.1016/j.jhazmat.2011.06.006

zinc oxide-modified mesoporous carbon CMK-3 called Zn-OCMK-3. The novelty of the present study consists of Taguchi optimization method for the removal of lead and mercury from aqueous solution and experimental data are presented in order to demonstrate the practical usage of zinc oxide-modified mesoporous carbon CMK-3. The optimum conditions with the higher pollutant removal efficiency (PRE) for batch adsorption studies were determined using the Taguchi method. In this study, agitation time, initial concentration, temperature, dose and pH were studied as the controllable factors. Accordingly, the percentage contribution of each aforementioned experimental parameter to the process is determined using the Taguchi method. Furthermore, Langmuir and Freundlich adsorption isotherms were studied to explain the sorption mechanism.

2. Design of experiments (DOE)

Design of experiments (DOE) is developing a scheme of experiment different conditions. The Taguchi method which was established by Genichi Taguchi has been generally adopted to optimize the design variables because this approach can significantly minimize the overall testing time and the experimental costs [28–31]. The Taguchi crossed array layout consists of an inner array and an outer array [32]. The inner array is made up of the orthogonal array (OA) selected from all possible combinations of the controllable factors. Using the orthogonal array specially designed for the Taguchi method, the optimum experimental conditions can be easily determined [28]. Accordingly, an analysis of the signal-to-noise (S/N) ratio is needed to evaluate the experimental results. Usually, three types of S/N ratio analysis are applicable: (1) lower is better (LB), (2) nominal is best (NB), and (3) higher is better (HB) [33]. Because the target of this study is to maximize the pollutant removal efficiency, the S/N ratio with HB characteristics is required, which is given by Eq. (1):

$$S/N = -10 \log_{10}\left[\frac{1}{n}\sum\left(\frac{1}{PRE_i}\right)^2\right] \quad (1)$$

where n is the number of repetitions under the same experimental conditions, and PRE represents the results of measurements.

3. Experimental

3.1. Materials

The reactants used in this study were tetraethyl orthosilicate (TEOS, 98%) as a silica source, distilled water (DW), Pluronic® P123 ($EO_{20}PO_{70}EO_{20}$) as a surfactant and phosphoric acid (H_3PO_4, 85%) from Aldrich (U.K.), sucrose as a carbon source, sodium hydroxide (NaOH), ethanol, sulfuric acid (H_2SO_4, 98%) and zinc nitrate tetrahydrate ($Zn(NO_3)_2{\cdot}4H_2O$) from Merck, Germany. Hydrochloric acid (HCl, 37%) and sodium hydroxide were used to control the pH of water samples.

3.2. Ordered mesoporous silica: SBA-15

SBA-15 was synthesized as reported by Colilla et al. [34]. The synthesis procedure was based on the use of P123 as directing agent of the silica and phosphoric acid as catalyst. The molar compositions of the initial solutions here presented are as follows: $SiO_2/P123/H_3PO_4/H_2O = 1/0.017/1.5/208$. These solutions were stirred at 35 °C for 24 h in sealed Teflon beakers and then further heated at 100 °C for 24 h. The obtained products were filtered, washed with DW and then dried at 90 °C for 12 h in air. The surfactant removal was done by heating first at 250 °C (3 h) and then at 550 °C (4 h) in air.

3.3. Ordered mesoporous carbon: CMK-3

CMK-3 was prepared according to the synthesis procedure described by Jun et al. [22]. SBA-15 was used as a hard template. 1 g SBA-15 was added to a solution obtained by dissolving 1.25 g of sucrose and 0.14 g of H_2SO_4 in 5 g H_2O. The resultant mixture was dried in an oven at 100 °C (6 h), and subsequently, the oven temperature was increased to 160 °C (6 h). After that, the SBA-15 containing the partially carbonizing organic masses was added in aqueous solution consisting sucrose (0.75 g), H_2SO_4 (0.08 g) and water (5 g). The resultant mixture was dried again at 100 °C (6 h), and subsequently, the oven temperature was increased to 160 °C (6 h). This powder sample was heated to 900 °C using a fused quartz reactor. The carbon–silica composite obtained was washed with 1 M aqueous ethanolic NaOH solution (50 vol.% NaOH solution and 50 vol.% ethanol) twice at 90 °C, in order to remove the silica template. The carbon samples obtained after the silica removal were filtered, washed with ethanol and dried at 120 °C.

3.4. Modification of CMK-3: OCMK-3

The texture and surface chemistry of synthesized CMK-3 was modified by HNO_3 to optimize their ability of dispersing active metal particles [35]. 0.1 g of dried CMK-3 powder was treated with 15 ml of HNO_3 solution (2 M) at 80 °C under refluxing. Samples were recovered and washed thoroughly with DW until the pH was close to 7. Finally, carbon supports were filtered, washed with distilled water and dried at 108 °C. It was denoted as OCMK-3.

3.5. Functionalization of OCMK-3: Zn-OCMK-3

The zinc oxide was loaded to the OCMK-3 by the equilibrium adsorption of Zn(II) ions from aqueous solution followed by calcination in air at 350 °C (2 h) to convert zinc nitrate to zinc oxide. The Zn(II) solution was prepared by dissolving $Zn(NO_3)_2.4H_2O$ in THF (1.5 mol/l). 80 ml of Zn(II) solution including 2 g of the OCMK-3 was agitated at 150 rpm for 3 days to reach the equilibrium state. The solid was separated by filtration and then dried in oven at 110 °C before calcinations at 350 °C. The ZnO functionalized OCMK-3 was referred as Zn-OCMK-3. The filtrate was analyzed by Inductively Coupled Plasma to ensure complete adsorption. It was observed that the Zn was taken up by OCMK-3.

3.6. Characterization

The X-ray powder diffraction (XRD) patterns were recorded on a Philips 1830 diffractometer using Cu Kα radiation. The diffractograms were recorded in the 2θ range of 0.5–10° with a 2θ step size of 0.01°. The surface area was measured by nitrogen adsorption/desorption at 77K using Brunaure–Emmet–Teller (BET) method. Scanning electron microscopy (SEM) images were obtained with JEOL 6300F SEM. Transmission electron microscopy (TEM) images for determination of ZnO dispersion and morphology of samples were obtained using a 300 kV Philips CM-30 TEM.

Table 1
Controllable factors and their levels.

Factor	Description	Level 1	Level 2	Level 3	Level 4
A	Agitation time (min)	10	30	120	240
B	Concentration (mg/l)	10	100	200	400
C	Dose (g/l)	0.1	0.3	0.5	0.7
D	Temperature (°C)	20	25	30	35
E	pH	2	4	6	7

3.7. Adsorption procedure

3.7.1. Optimization studies

This study considers five controllable factors, and each factor has four levels (Table 1). Therefore, an L_{16} (4^5) orthogonal array is chosen, and the experimental conditions (Table 2) can be obtained by combining Table 1 and the L_{16} (4^5) orthogonal array. Stock solutions of 1000 mg/l Pb(II) and Hg(II) were prepared from $Pb(NO_3)_2$ as the Pb source and $Hg(NO_3)_2$ as the Hg source in deionized water. A series of aqueous solutions of Pb and Hg with the agitation time of 10–240 min, initial concentration of 10–400 mg/l, dose of 0.1–0.7 g/l, temperature of 20–35 °C, and pH of 2–7 were prepared (Table 2). Batch adsorption tests were performed by shaking 500 ml Amber Winchester bottles containing 100 ml of the Pb(II) and Hg(II) in a Gallenkamp incubator shaker, stirring at 150 rpm. The concentration of heavy metal in the supernatant was analyzed with an Inductively Coupled Plasma Atomic Emission Spectrometer (ICP-AES – Perkin-Elmer 4300 DV Model). The PRE is calculated using Eq. (2):

$$\mathrm{PRE} = \left(\frac{C_0 - C_e}{C_0}\right) \times 100 \tag{2}$$

where C_0 and C_e are the initial and equilibrium concentrations of pollutant (mg/l), respectively.

The analysis of mean (ANOM) statistical approach is adopted herein to develop the optimal conditions [31]. Initially, the mean of the S/N ratio of each factor at a certain level should be calculated. For example, $(M)\overset{\text{Level}=i}{\text{Factor}} = I$, the mean of the S/N ratio of factor I in level i, is given by Eq. (3):

$$(M)\overset{\text{Level}=i}{\text{Factor}} = I = \frac{1}{n_{Ii}} \sum_{j=1}^{n_{Ii}} \left[\left(\frac{S}{N}\right) \overset{\text{Level}=i}{\text{Factor}} = I \right]_j \tag{3}$$

where n_{Ii} represents the number of appearances of factor I in the level i, and $[(S/N)\overset{Level=i}{Factor} = I]_j$ is the S/N ratio of factor I in level i, and its appearance sequence in Table 2 is the jth. By the same measure, the mean of the S/N ratios of the other factors in a certain level can be determined. Thereby, the S/N response table is obtained, and the optimal conditions are established. Finally, the confirmation experiments on solidification under these optimal conditions are carried out. In addition to ANOM, the analysis of variance (ANOVA) [31] statistical method is also used to analyze the influence of each controllable factor on removal of lead and mercury. The percentage contribution of each factor, R_F, is given by Eq. (4):

$$R_F = \frac{SS_R - (DOF_R V_{ER})}{SS_T} \times 100 \tag{4}$$

In Eq. (4), DOF_R represents the degree of freedom for each factor, which is obtained by subtracting one from the number of the level of each factor (L). The total sum of squares, SS_T, is given by Eq. (5):

$$SS_T = \sum_{j=1}^{m} \left(\sum_{j=1}^{n} \mathrm{PRE}_i^2 \right) - mn(\overline{\mathrm{PRE}}_T)^2 \tag{5}$$

where $\overline{\mathrm{PRE}}_T = \Sigma_{j=1}^{m}(\Sigma_{i=1}^{n}\mathrm{PRE}_i)_j/(mn)$, m represents the number of experiments carried out in this study, and n represents the number of repetitions. The factorial sum of squares, SS_F, is given by Eq. (6):

$$SS_F = \frac{mn}{L} \sum_{k=l}^{L} \left(\overline{\mathrm{PRE}}_k^F - \overline{\mathrm{PRE}}_T \right)^2 \tag{6}$$

where $\overline{\mathrm{PRE}}_k^F$ is the average value of the measurement results of a certain factor in the kth level.

Additionally, the variance of error, V_{Er}, is given by Eq. (7):

$$V_{Er} = \frac{SS_T - \sum_{F=A}^{E} SS_F}{m(n-1)} \tag{7}$$

3.7.2. Sorption isotherm studies

For sorption isotherm studies, a series of aqueous solutions of lead and mercury with the initial concentration of 10, 100, 200 and 400 mg/l, were prepared. The experiments were carried out under stirring at 150 rpm at temperature of 25 °C for 120 min contact time, dose 0.5 g/l Zn-OCMK-3 and pH 6. The amount of lead and mercury adsorption at equilibrium, q_e (mg/g) was calculated by Eq. (8):

$$q_e = \frac{C_0 - C_e}{W} V \tag{8}$$

where C_0 and C_e (mg/g) are the liquid phase initial and equilibrium concentrations of the heavy metals respectively. V is the volume of the solution (l), and W is the mass of dry adsorbent used (g) [36]. The sorption equilibrium data of Pb(II) and Hg(II) onto the

Table 2
The S/N ratio of each test.

Tests	Factor					*PRE* (%)				S/N	
						Pb(II)		Hg(II)			
	A	B	C	D	E	PRE_1	PRE_2	PRE_1	PRE_2		Hg(II)
Tests 1	10	10	0.1	20	2	28.00	28.30	30.50	30.38	28.98	29.66
Tests 2	10	100	0.3	25	4	31.00	28.74	35.75	35.50	29.48	31.03
Tests 3	10	200	0.5	30	6	63.00	63.01	47.54	47.95	35.98	33.57
Tests 4	10	400	0.7	35	7	48.40	46.50	47.20	47.10	33.51	33.46
Tests 5	30	10	0.3	30	7	65.50	65.35	74.25	74.13	36.31	37.40
Tests 6	30	100	0.1	35	6	55.50	55.45	55.50	55.00	34.88	34.84
Tests 7	30	200	0.7	20	4	32.50	32.49	45.50	45.40	30.23	33.15
Tests 8	30	400	0.5	25	2	26.60	26.00	35.00	35.30	28.39	30.91
Tests 9	120	10	0.5	35	4	78.50	78.35	97.20	97.00	37.88	39.74
Tests 10	120	100	0.7	30	2	68.50	66.30	51.50	51.40	36.56	34.22
Tests 11	120	200	0.1	25	7	51.00	51.10	45.50	45.74	34.15	33.18
Tests 12	120	400	0.3	20	6	41.00	41.10	43.00	43.50	32.26	32.71
Tests 13	240	10	0.7	25	6	95.75	95.75	97.40	97.67	**39.62**	**39.78**
Tests 14	240	100	0.5	20	7	68.00	68.98	64.00	64.00	36.71	36.12
Tests 15	240	200	0.3	35	2	48.50	48.00	34.10	34.14	33.66	30.66
Tests 16	240	400	0.1	30	4	32.70	32.60	45.00	43.40	30.27	32.90

PRE_1 and PRE_2 for both pollutants represent the pollutant removal efficiency at first and second test pieces, respectively. The boldfaces correspond to the maximum value of S/N ratio among the 16 tests.

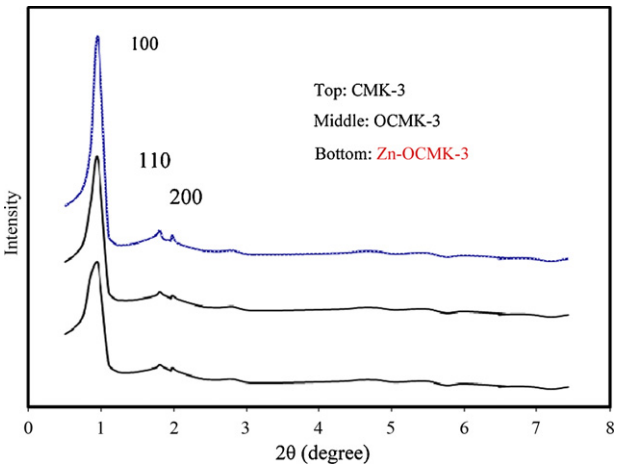

Fig. 1. XRD patterns of CMK-3, OCMK-3 and Zn-OCMK-3.

Zn-OCMK-3 were analyzed in terms of Langmuir and Freundlich isotherm models [37]. The Langmuir model is given by Eq. (9):

$$\frac{C_e}{q_e} = \left(\frac{1}{q_m b}\right) + \left(\frac{1}{q_m}\right) C_e \quad (9)$$

where q_e and C_e are the equilibrium concentrations of metal ions in the adsorbed and liquid phases in mg/g and mg/l, respectively. q_m (mg/g) and b (l/mg) are the Langmuir constants. In other word, q_m is the maximum monolayer capacity and b is the adsorption affinity onto the adsorption sites and it is related to energy of adsorption. The Langmuir constants can be calculated from the slope and intercept of the linear plot, C_e/q_e versus C_e. The essential characteristics of the Langmuir isotherm can also be expressed in terms of a dimensionless constant of separation factor or equilibrium parameter, R_L, which is defined as

$$R_L = \frac{1}{1 + C_0 b} \quad (10)$$

where b is the Langmuir constant and C_0 is the initial concentration of metal ions. The R_L value indicates the shape of isotherm

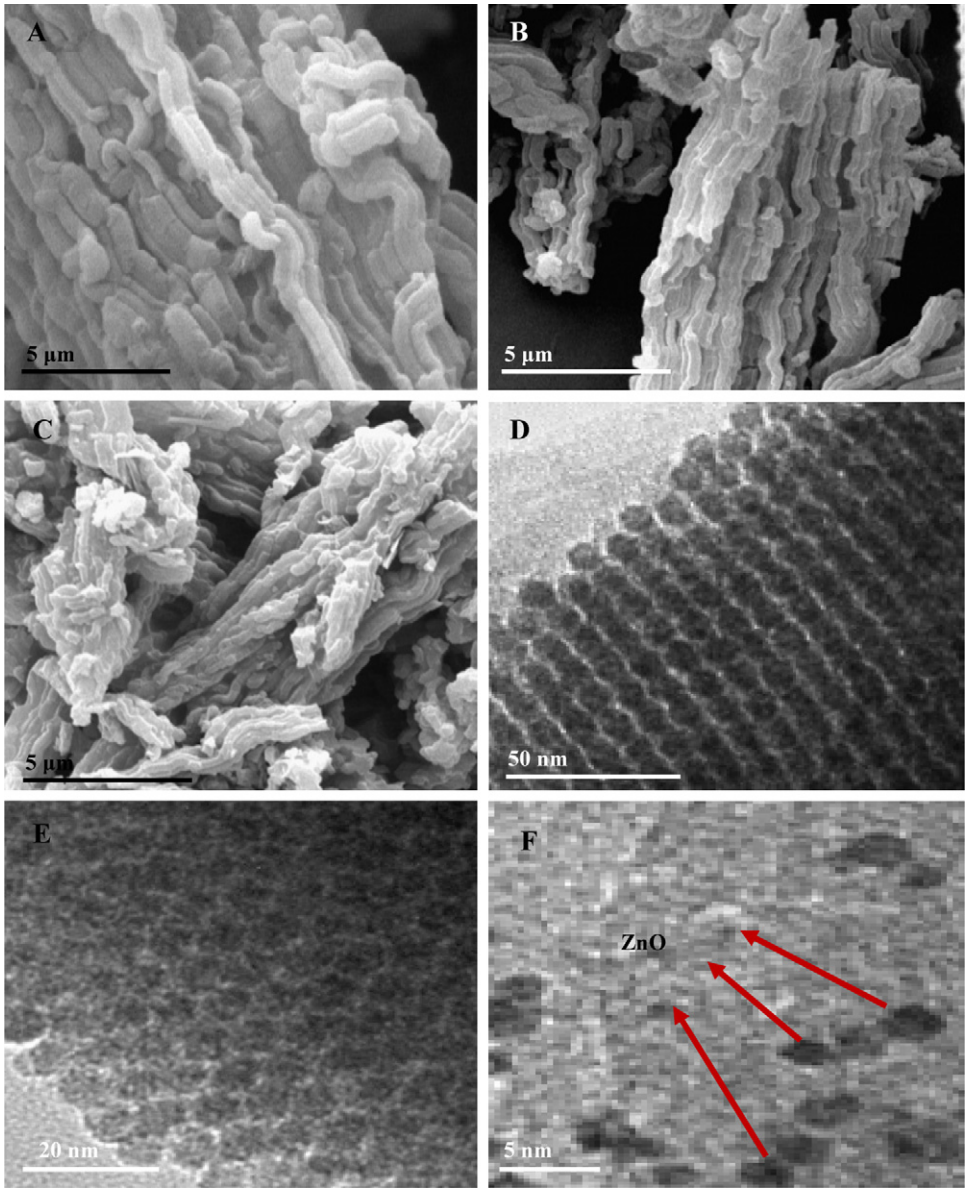

Fig. 2. Images of samples. (A) SBA-15: SEM, (B) CMK-3: SEM, (C) ZnO supported on OCMK-3 (Zn-OCMK-3): SEM, (D) hexagonal structure of CMK-3: TEM, (E) oxidized mesoporous carbon (OCMK-3): TEM (F) zinc oxide-modified mesoporous carbon (Zn-OCMK-3): TEM.

Table 3
S/N ratio response table for Pb(II).

Factor/level	$[(S/N)^{Level}_{Factor}]_j$				$(M)^{Level}_{Factor}$
	$j=1$	$j=2$	$j=3$	$j=4$	
A/1	28.98	29.48	35.98	33.51	32.00
A/2	36.31	34.88	30.23	28.39	32.46
A/3	37.88	36.56	34.15	32.26	**35.22**
A/4	39.62	36.71	33.66	30.27	35.07
B/1	28.98	36.31	37.88	39.62	**35.70**
B/2	29.48	34.88	36.56	36.71	34.41
B/3	35.98	30.23	34.15	33.66	33.51
B/4	33.51	28.39	32.26	30.27	31.12
C/1	28.98	34.88	34.15	30.27	32.08
C/2	29.48	36.31	32.26	33.66	32.93
C/3	35.98	28.39	37.88	36.71	34.75
C/4	33.51	30.23	36.56	39.62	**34.99**
D/1	28.98	30.23	32.26	36.71	32.05
D/2	29.48	28.39	34.15	39.62	32.92
D/3	35.98	36.31	36.56	30.27	34.79
D/4	33.51	34.88	37.88	33.66	**34.99**
E/1	28.98	28.39	36.56	33.66	31.91
E/2	29.48	30.23	37.88	30.27	31.97
E/3	35.98	34.88	32.26	39.62	**35.69**
E/4	33.51	36.31	34.15	36.71	35.18

The boldface corresponds to the maximum value of the mean of the S/N ratios of a certain factor among the four levels.

Table 4
S/N ratio response table for Hg(II).

Factor/level	$[(S/N)^{Level}_{Factor}]_j$				$(M)^{Level}_{Factor}$
	$j=1$	$j=2$	$j=3$	$j=4$	
A/1	29.66	31.03	33.57	33.46	31.94
A/2	37.40	34.84	33.15	30.91	34.08
A/3	39.74	34.22	33.18	32.71	**34.97**
A/4	39.78	36.12	30.66	32.90	34.87
B/1	29.66	37.40	39.74	39.78	**36.65**
B/2	31.03	34.84	34.22	36.12	34.06
B/3	33.57	33.15	33.18	30.66	32.64
B/4	33.46	30.91	32.71	32.90	32.50
C/1	29.66	34.84	33.18	32.90	32.65
C/2	31.03	37.40	32.71	30.66	32.96
C/3	33.57	30.91	39.74	36.12	35.09
C/4	33.46	33.15	34.22	39.78	**35.16**
D/1	29.66	33.15	32.71	36.12	32.92
D/2	31.03	30.91	33.18	39.78	33.73
D/3	33.57	37.40	34.22	32.90	34.53
D/4	33.46	34.84	39.74	30.66	**34.68**
E/1	29.66	30.91	34.22	30.66	31.37
E/2	31.03	33.15	39.74	32.90	34.21
E/3	33.57	34.84	32.71	39.78	**35.23**
E/4	33.46	37.40	33.18	36.12	35.05

The boldface corresponds to the maximum value of the mean of the S/N ratios of a certain factor among the four levels.

[38]. R_L values between 0 and 1 indicate favorable adsorption, while $R_L > 1$, $R_L = 1$, and $R_L = 0$ indicate unfavorable, linear, and irreversible adsorption isotherms. Also, the Freundlich model is given by Eq. (11):

$$\ln \quad q_e = \ln \quad k_f + \left(\frac{1}{n}\right) \ln \quad C_e \tag{11}$$

where q_e and C_e are the equilibrium concentrations of metal ions in the adsorbed and liquid phases in mg/g and mg/l, respectively. k_f (mg/g) and n (l/mg) are the Freundlich constants which are related to the sorption capacity and intensity, respectively. The Freundlich constants k_f and n can be calculated from the intercept and slope of the linear plot with $\ln q_e$ versus $\ln C_e$.

4. Results and discussion

4.1. Characterization

4.1.1. XRD patterns and BET surface area

The XRD of synthesized samples are shown in Fig. 1. The XRD patterns of CMK-3 showed three diffraction peaks that can be indexed to (100), (110), and (200) in the 2θ range from 0.5° to 10°, representing well-ordered hexagonal mesopores [22]. The XRD patterns show well-resolved reflections indicating that CMK-3 nicely maintains its original structure even after the modification with HNO_3 and functionalization with ZnO. CMK-3 had porous structure and high surface area (998 m^2/g) which can accommodate ZnO in a spreading manner, the ZnO connects to the carbon surface via oxygen atoms. The lower surface area of OCMK-3 (985 m^2/g) compared with pure CMK-3 is mainly attributed to the presence of dense carboxylic surface groups. It is considered that calcination at 350 °C makes the Zn(II) ions adsorbed on the carbon bind to the mesoporous carbon via oxygen atoms upon the formation of zinc oxide, in which the surface area of Zn-OCMK-3 also may progressively increase (1030 m^2/g).

4.1.2. SEM and TEM images

SEM images of the synthesized samples are shown in Fig. 2A–C. Fig. 2A reveals that the SBA-15 sample consists of many rope-like domains with relatively uniform sizes of ≈1 μm, which are aggregated into wheat-like macrostructures. The preservation of rope-like morphology during the SBA-15 templating synthesis of CMK-3 from sucrose provides additional confirmation that carbon is faithful replica of the SBA-15 (Fig. 2B). Furthermore, the carbon replica possesses the same wheat-like shape similar to the SBA-15. Fig. 2C is the SEM picture of the ZnO particle on CMK-3. TEM image showed in Fig. 2D confirm that the structure of CMK3 is well-ordered hexagonal arrays of mesopores. Fig. 2E shows that after oxidation treatment, ordered structure is maintained. Fig. 2F clearly demonstrates the ZnO particulates deposited in the pores of the carbon. As it can be seen, ZnO is well dispersed on the carbon support.

4.2. Optimization

4.2.1. Optimum conditions

The pollutant removal efficiency in Tests 1–16 measured for Pb(II) and Hg(II) according to the method and Eq. (2) (Table 2). Substituting the number of experimental repetitions and results of the measurement (PRE) into Eq. (1), the S/N ratio of each test condition are determined (Table 2). The boldfaces in Table 2 refer to the maximum value of S/N ratio among the 16 tests. Subsequently, the values of the S/N ratio were substituted into Eq. (3) and the mean of the S/N ratios of a certain factor in the ith level, $(M)^{Level}_{Factor}$, was obtained (Table 3 (Pb) and Table 4 (Hg)). The $(M)^{Level}_{Factor}$ shows the effect of each level of each factor on the response, independently. It is calculated by averaging the S/N ratio values of all the experiments where the level of that factor has been used. In Tables 3 and 4 the boldfaces refer to the maximum value of the mean of the S/N ratios of a certain factor among four levels, and thus it indicates the optimum conditions for adsorption process. From these Tables, the optimum conditions for removal of Pb(II) and Hg(II) are as follows: (1) The agitation time is 120 min; (2) the initial concentration is 10 mg/l; (3) the temperature is 35 °C; (4) the dose is 0.7 g/l; and (5) the pH is 6. The confirmation experiment was carried out according to the aforementioned optimum conditions, the PRE of Pb and Hg registered, and the S/N ratio was calculated (Table 5). The value of the S/N ratio under optimum conditions (Pb: 39.75 and Hg: 39.91) slightly exceeds that in Test 13 (Pb: 39.62 and Hg: 39.78), and the average PRE under optimum conditions (Pb: 97.25% and Hg: 99%) indeed exceeds that in Test 13 (Pb: 95.75% and Hg: 97.54%). Although the difference of the S/N ratio between the optimum conditions and

Table 5
The optimum conditions for Pb(II) and Hg(II) adsorption.

	A	B	C	D	E	PRE_1	PRE_2	S/N
Test 13 for Pb(II)	240	10	0.7	25	6	95.75	95.75	39.62
Optimization condition for Pb(II)	120	10	0.7	35	6	97.00	97.50	39.75
Test 13 for Hg(II)	240	10	0.7	25	6	97.40	97.67	39.78
Optimization condition for Hg(II)	120	10	0.7	35	6	98.50	99.50	39.91

PRE_1 and PRE_2 for both pollutants represent the pollutant removal efficiency at first and second test pieces, respectively.

Test 13 is very little, the agitation time substantially decreases from 4 h (Test 13) to 2 h (optimum conditions). Furthermore, the PRE increases from 95.75 to 97.25% and from 97.54 to 99% for Pb(II) and Hg(II), respectively. These results are pretty exciting due to the fact the lower agitation time corresponds to a better adsorption system.

4.2.2. Agitation time

The $(M)_{\text{Factor}}^{\text{Level}}$ are shown in Figs. 3–7 for the experimental conditions proposed by Taguchi method. Fig. 3 shows the effect of agitation time on the S/N ratio in the removal of Pb(II) and Hg(II). The distribution of adsorbate between adsorbent and solution is influenced by agitation time. It is seen that the time required for equilibrium is 120 min. In the other words, the optimum time is 2 h. This is obvious from the fact that a large number of vacant surface sites are available for the adsorption during the initial stage and with the passage of time, the remaining vacant surface sites are difficult to be occupied due to repulsive forces between the solute molecules on the solid phase and in the bulk liquid phase. Heavy metal adsorption slightly decreases after 120 min. It may be related to desorption process at upper time.

4.2.3. Initial concentration

Fig. 4 shows that the S/N for Pb concentration decreases from 35.70 to 31.12 by increasing concentration from 10 to 400 mg/l and the S/N for Hg concentration decreases from 36.65 to 32.50 by increasing concentration from 10 to 400 mg/l. The efficiency of metal removal is affected by the initial metal concentration, with the removal percentage decreases as the concentration increases. This effect has been attributed to the surface binding of low-affinity surface sites as high-affinity ones begin to reach saturation, leading to a reduction in the removal efficiency. Seco et al. [39] have reported that the amount of adsorption was decreased with the increase in initial concentration.

4.2.4. Adsorbent amount

The present study shows that the Zn-OCMK-3 is an effective adsorbent for the removal of Pb(II) and Hg(II) from aqueous solution (97.25% for Pb and 99% for Hg). It can be seen from Fig. 5 that the dose for Pb(II) and Hg(II) was increased with the increase in adsorbent. Amount of Zn-OCMK-3 was varied from 0.1 to 0.7 g/l. It is apparent that the equilibrium concentration in solution phase decreases with increasing carbonous adsorbents amount for a given initial Pb(II) and Hg(II) concentration. Since the amount of metals removed from the aqueous phase increases as the sorbent amount is increased in the batch vessel with a fixed initial heavy metal concentration. This result was anticipated because for a fixed initial solute concentration, increasing amount of adsorbent provides greater surface area.

4.2.5. Temperature

The plot of adsorption capacity as a function of temperature is shown in Fig. 6. The uptake of Pb and Hg onto the Zn-OCMK-3 increased with increase in temperature from 20 to 35 °C, indicating more chemical interaction between the sorbate and the surface functionalities of the Zn-OCMK-3. Adsorption efficiency is observed to increase on raising the temperature, as previously reported [40,41]. Seco et al. [39] have investigated the adsorption of heavy metals onto activated carbon. They concluded that increase in temperature results in greater removal efficiency. The adsorption of Pb(II) onto another carbon material has been reported by Wang et al. [42]. In their study, the Pb(II) adsorption capacity increased with the rise of temperature.

4.2.6. Solution pH

One of the critical parameter in the treatment of heavy metals by the sorption medium is pH, because the surface charge of an adsorbent could be modified by changing pH of the solution. Fig. 7 shows that the S/N ratio increased with the pH value from 2 to 6. The removal of Pb(II) and Hg(II) from water by Zn-OCMK-3 was found to be dependent on the solution pH value. This can be explained on the basis of Surface Complex Formation (SCF) theory [39]. In the SCF theory, adsorption of inorganic species onto hydrous solids is described as a chemical coordination and electrostatic process involving specific interactions at the solid/solution interface. The increase in the metal removal as the pH increases is on the basis of a decrease in competition between proton and metal species for the surface sites, and by the decrease in positive surface charge, which results in a lower coulombic repulsion of the sorbing metal.

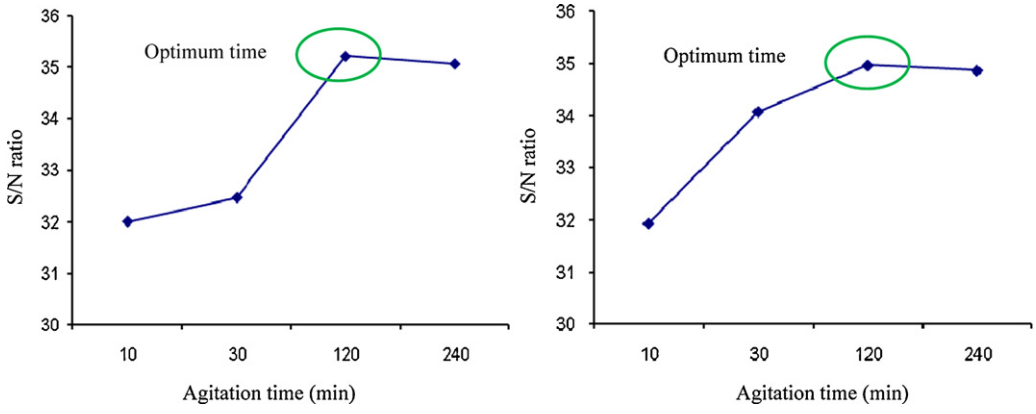

Fig. 3. The effect of agitation time on the S/N ratio in the removal of Pb(II) (left) and Hg(II) (right). Circles on figures indicate optimum time for adsorption process.

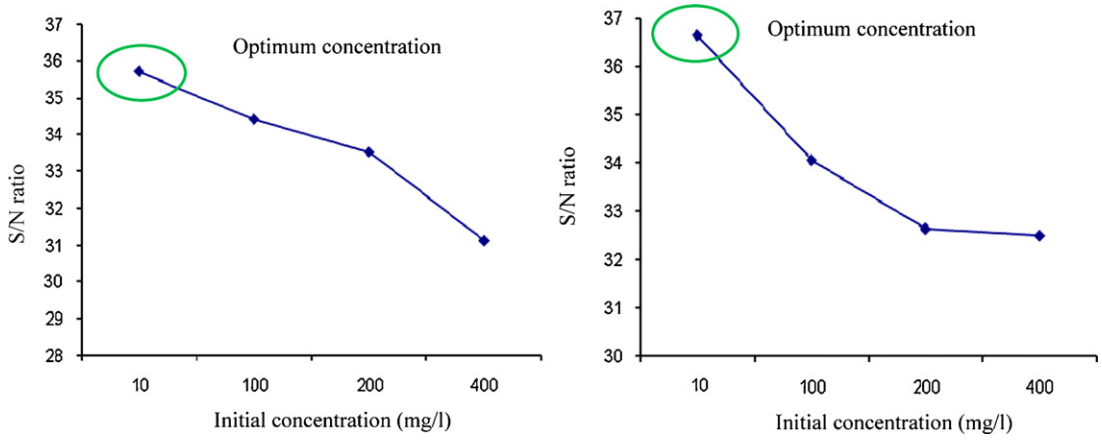

Fig. 4. The effect of initial concentration on the S/N ratio in the removal of Pb(II) (left) and Hg(II) (right). Circles on figures indicate optimum concentration for adsorption process.

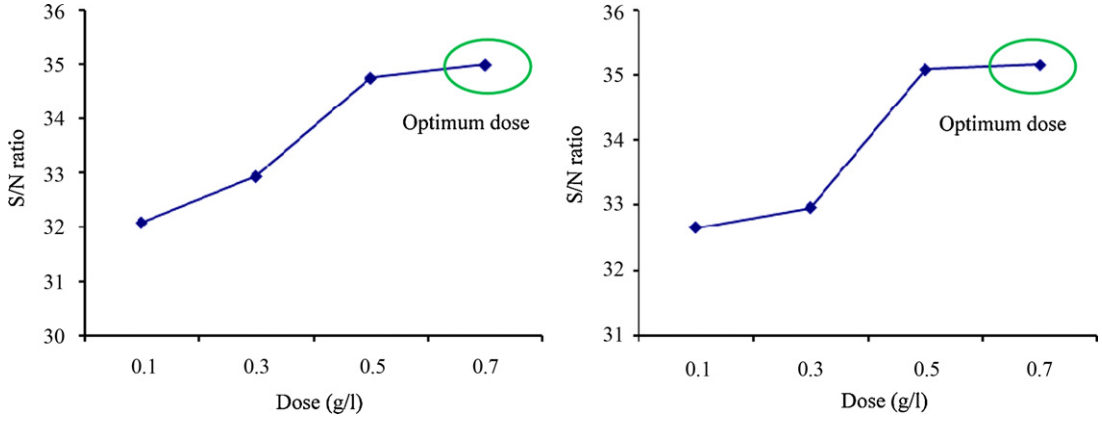

Fig. 5. The effect of adsorbent dose on the S/N ratio in the removal of Pb(II) (left) and Hg(II) (right). Circles on figures indicate optimum dose for adsorption process.

At pH 2, adsorption is very weak due to the competition of H_3O^+. At higher pH increase of pH of the aqueous solution leads to the hydrolysis of Pb and Hg species. The surface functional groups may exchange a proton with positively charged Pb(II) and Hg(II) species in aqueous solution. The mechanism of Pb and Hg retention on Zn-OCMK-3, can be described by the adsorption reactions as following expressions:

$$Zn\text{–}OH + Pb^{2+} \rightarrow Zn\text{–}O\text{–}Pb^{+} + H^{+} \quad (a)$$

$$Zn\text{–}OH + PbOH^{+} \rightarrow Zn\text{–}O\text{–}Pb(OH) + H^{+} \quad (b)$$

$$Zn\text{–}OH + Hg^{2+} \rightarrow Zn\text{–}O\text{–}Hg + H^{+} \quad (c)$$

$$Zn\text{–}OH + HgOH^{+} \rightarrow Zn\text{–}O\text{–}Hg(OH) + H^{+} \quad (d)$$

Tamura and Furuichi [43] have examined the adsorption of heavy metals onto MnO_2 and Fe_2O_3, and have concluded that surface hydroxyl groups contribute to the binding of heavy metals for the metal oxide. The point of zero charge (pH_{zpc}) plays an important role in the adsorption process. The pH_{zpc} of Zn-OCMK-3 was found to be 4.8. At pH above pH_{zpc}, the surface of mesoporous carbon is negative and there is a strong electrostatic attraction between surface groups and Pb(II) and Hg(II) species. As a result, above pH_{zpc},

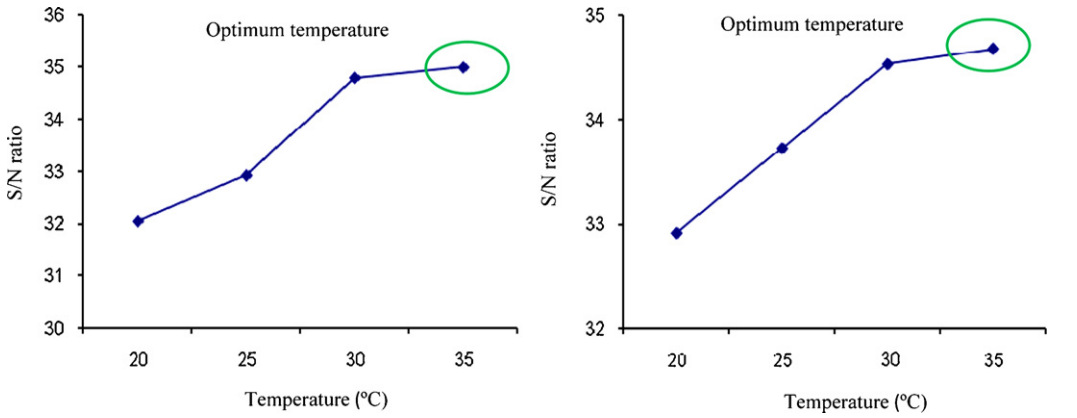

Fig. 6. The effect of temperature on the S/N ratio in the removal of Pb(II) (left) and Hg(II) (right). Circles on figures indicate optimum temperature for adsorption process.

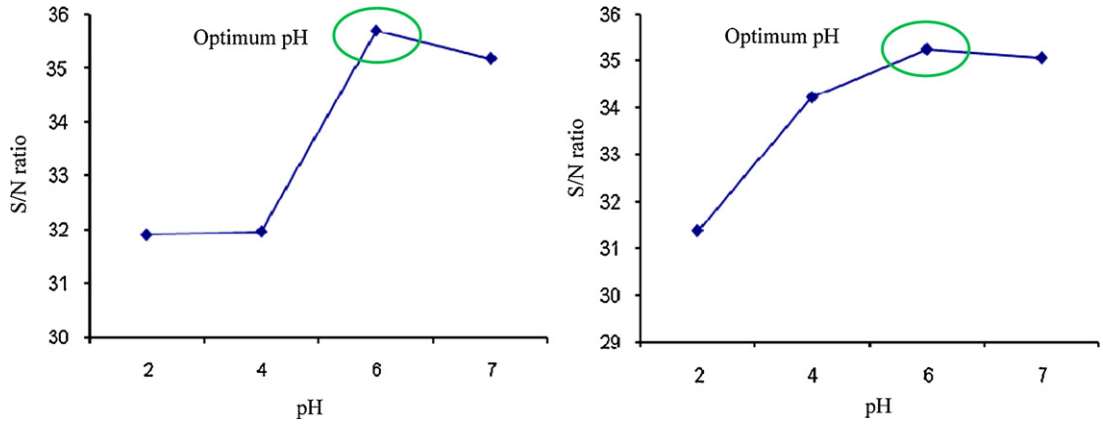

Fig. 7. The effect of pH on the S/N ratio in the removal of Pb(II) (left) and Hg(II) (right). Circles on figures indicate optimum pH for adsorption process.

Table 6
The average of the measurement results of a certain factor in the *k*th level ($\overline{PRE}_K^A$, $\overline{PRE}_K^B$, $\overline{PRE}_K^C$, $\overline{PRE}_K^D$, $\overline{PRE}_K^E$) and the average of total PRE (PRE_T) for Pb(II) and Hg(II).

Pollutant	Level	$\overline{PRE}_K^A$	$\overline{PRE}_K^B$	$\overline{PRE}_K^C$	$\overline{PRE}_K^D$	$\overline{PRE}_K^E$	$\overline{PRE}_T$
Pb(II)	Level 1	42.119	66.938	41.831	42.546	42.525	51.952
	Level 2	44.924	55.309	46.149	50.743	43.360	
	Level 3	59.481	48.700	59.055	57.120	63.820	
	Level 4	61.285	36.863	60.774	57.400	58.104	
Hg(II)	Level 1	40.240	74.816	43.878	45.785	37.790	53.017
	Level 2	52.510	51.581	46.796	53.483	55.594	
	Level 3	59.355	43.234	60.999	54.396	60.945	
	Level 4	59.964	42.438	60.396	58.405	57.740	

the adsorption of Pb(II) and Hg(II) was found to be high. At pH values less than pH_{zpc}, the carbon surface is positively charged resulting in lower adsorption due to electrostatic repulsion between the positive surface charge of mesoporous carbon and Pb^{2+} and Hg^{2+}.

4.3. Percentage of contribution

Initially, PRE_k^F (the average value of the measurement results of a certain factor in the *k*th level) was obtained from PRE_i in Table 2 and these are listed in Table 6. By substituting PRE_k^F and PRE_T (for Pb = 51.952 and for Hg = 53.017) into Eq. (6), the factorial sum of squares, SS_F, for each factor was calculated individually and these are listed in Table 7. Using Eq. (5), the total sum of squares, SS_T, was determined. By substituting SS_F and SS_T (for Pb = 12136.851 and for Hg = 12677.203) in Eq. (7), the variance of error, V_{Er}, was obtained. Finally, by the substitution of SS_F, SS_T, V_{Er} (for Pb = 0.517 and for Hg = 0.153), and $DOF_F = 3$ in Eq. (4), the percentage contribution of each factor, R_F, was determined sequentially; and these values are presented in Table 7. According to their magnitudes, the rank order of the percentage contributions of each factor for lead and mercury is as follows: (1) the initial concentration (Pb: 31.238% and Hg: 43.221%), (2) the agitation time (Pb: 19.095% and Hg: 15.899%), (3) the pH of solution (Pb: 22.490 and Hg: 20.425%), (4) the dose of adsorbent (Pb: 17.414% and Hg: 15.170%), and (5) the temperature of solution (Pb: 9.632% and Hg: 5.266%). The initial concentration is the most influential factor on the adsorption process among the five factors. For example, as the initial concentration of mercury is 10 mg/l, the average of pollutant removal efficiencies in Test 1, Test 5, Test 9, and Test 13 are 30.44, 74.19, 97.10, and 96.58%, respectively, and the average of all of them is 74.58%. In addition to, as the initial concentration of mercury is 400 mg/l, the average of pollutant removal efficiencies in Test 4, Test 8, Test 12, and Test 16 are 47.15, 35.15, 43.25, and 44.20%, respectively, and the average of all of them is 42.44%. In other words, pollutant removal efficiency in the initial concentration of 10 mg/l was about 2 times as much of the initial concentration of 400 mg/l, whereas pollutant removal efficiency at the temperature (the least influential factor) of 35 °C was only 1.2 times as much of the temperature of 20 °C.

4.4. Adsorption isotherms

The relationship between the amount of a substance adsorbed per unit mass of adsorbent at constant temperature and its concentration in the equilibrium solution is called the adsorption isotherm. The equilibrium adsorption isotherms are important in determining the adsorption capacity of metal ions and diagnose the mechanism of adsorption onto the Zn-OCMK-3. The sorption data were fitted to Langmuir and Freundlich isotherm models described in Section 3.7.2. Langmuir and Freundlich isotherm models correspond to homogeneous and heterogeneous adsorbent surfaces, respectively [37]. As can be seen from the isotherms in Fig. 8 and regression coefficients in Table 8, the Langmuir model shows the best fit compared to Freundlich model. Maximum adsorption

Table 7
Determination of percentage contribution of each factor.

Pollutant	Factor	DOF_F	SS_F	R_F (%)	SS_T	V_{Er}
Pb(II)	Agitation time; A	3	2319.069	19.095	12136.851	0.517
	Concentration; B	3	3792.812	31.238		
	Dose; C	3	2115.065	17.414		
	Temperature; D	3	1170.560	9.632		
	pH; E	3	2731.074	22.490		
Hg(II)	Agitation time; A	3	2015.491	15.899	12677.203	0.153
	Concentration; B	3	5479.252	43.221		
	Dose; C	3	1923.119	15.170		
	Temperature; D	3	667.611	5.266		
	pH; E	3	2589.289	20.425		

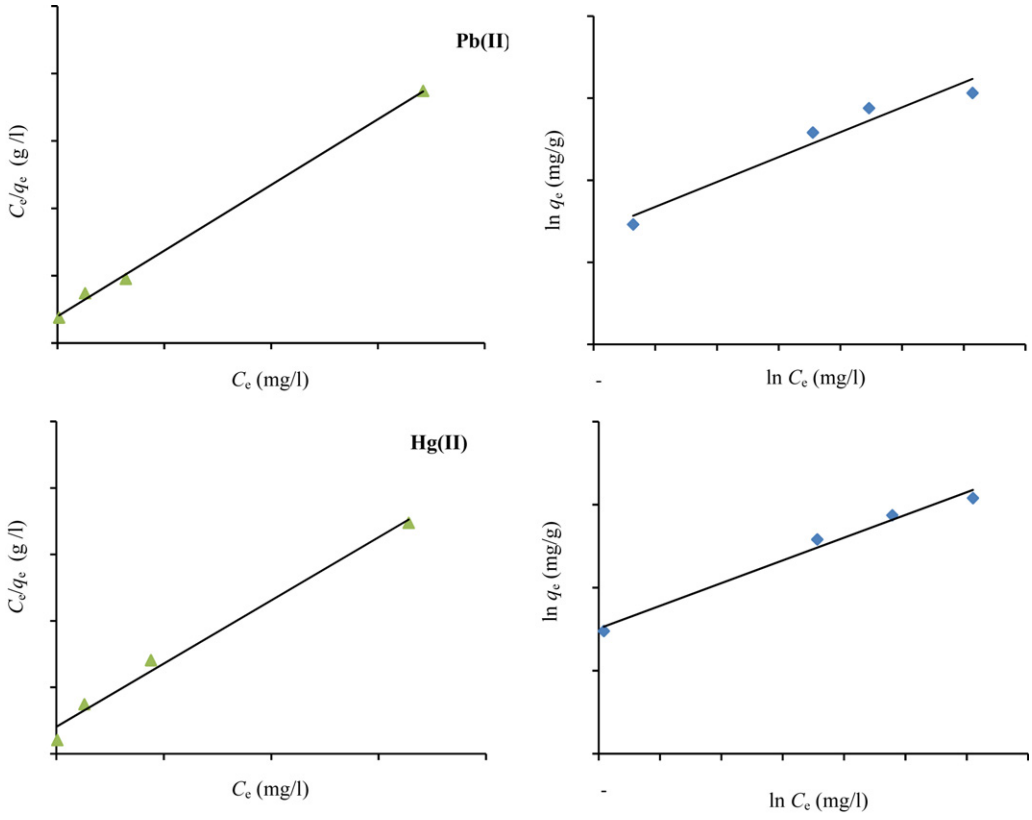

Fig. 8. Langmuir (left figures) and Freundlich (right figures) isotherms for Pb(II) and Hg(II) adsorption onto Zn-OCMK-3.

Table 8
Langmuir and Freundlich parameters for adsorption of Pb(II) and Hg(II) on Zn-OCMK-3.

Heavy metals	Langmuir			Freundlich		
	q_m (mg/g)	b (l/mg)	R^2	K_f (mg/g)	n (l/mg)	R^2
Pb(II)	500.00	0.051	0.998	28.62	1.650	0.947
Hg(II)	526.31	0.047	0.986	35.27	1.828	0.983

capacities of Pb(II) and Hg(II) by the Zn-OCMK-3 expressed by Langmuir coefficient q_m demonstrates that adsorption capacity increased in the sequence, Pb(II) [500 mg/g] < Hg(II) [526.31 mg/g], which is in the same order of increasing hydrated radius of heavy metals studied. The removal order of preference for the two metals was also the same as those revealed by Kadirvelu et al. [44]. The dimensionless parameter (R_L) value, which is defined in Eq. (10) described above can be computed by substituting the values of b and C_0 to the equation. The R_L values were 0.24 for Pb(II) and 0.25 for Hg(II). For the two metal ions the values of R_L were between 0 and 1, pointing out the favorable adsorption onto the Zn-OCMK-3. Freundlich coefficient K_f, which represents the adsorption capacity was found to be increased in the sequence, Pb(II) [28.62 mg/g] < Hg(II) [35.27 mg/g], which is the same as that revealed by Langmuir coefficient q_m (Table 8).

5. Conclusions

Using zinc oxide-modified CMK-3 (Zn-OCMK-3) and the Taguchi method, this investigation has studied the optimum conditions for Pb and Hg adsorption from water. The optimum conditions for removal of Pb(II) and Hg(II) are the agitation time of 120 min, the initial concentration of 10 mg/l, the temperature of 35 °C, the dose of 0.7 g/l, and the pH of 6. Based on the experimental results for Zn-OCMK-3, it can be deduced that this nanoporous carbon is very effective in removing the lead and mercury with a high PRE (97.25% for Pb(II) and 99% for Hg(II) under optimum condition). Removal of lead and mercury were highly concentration dependent. Number of Pb and Hg ions highly increase from initial concentration of 10–400 mg/l. At high concentration, a lot of ions cannot be adsorbed, leading to a significant reduction in the removal efficiency. The Langmuir model shows the best fit compared to Freundlich model. Therefore, the adsorption process can be described by the formation of monolayer coverage of the adsorbate on the adsorbent surface.

Acknowledgment

We are grateful to appreciate to the Iran Nanotechnology Initiative Council for financing this work.

References

[1] J.L. Zhou, S.M. Salvador, Y.P. Liu, M. Sequeria, Heavy metals in the tissues of dolphins (*Delphinus delphis*) stranded on the Portuguese coast, Sci. Total Environ. 273 (2001) 61–76.
[2] J. Goel, K. Kadirvelu, C. Rajagopal, V.K. Garg, Removal of lead(II) by adsorption using treated granular activated carbon: batch and column studies, J. Hazard. Mater. 125 (2005) 211–220.
[3] K. Warfivinge, Mercury exposure of a female dentist before pregnancy, Br. Dent. J. 178 (1995) 149–152.
[4] G. Zolfaghari, A. Esmaili-sari, S.M. Ghasempouri, B. Hassanzade Kiabi, Examination of mercury concentration in the feather of 18 species of birds in southwest Iran, Environ. Res. 104 (2007) 258–265.
[5] G. Zolfaghari, A. Esmaili-sari, S.M. Ghasempouri, B. Hassanzade Kiabi, R. Rajabi Baydokhti, Multispecies monitoring study about bioaccumulation of mercury in Iranian birds (Khuzestan to Persian Gulf): effect of taxonomic affiliation, trophic level and feeding habitat, Environ. Res. 109 (2009) 830–836.
[6] NCAP, National Caspian Action Plan, Caspian Environment Program, Islamic Republic of Iran, 2002.
[7] A. Ndabigengesere, K.S. Narasiah, Quality of water treated by coagulation using Moringa oleifera seeds, Water Res. 32 (1998) 781–791.

[8] X. Hu, F.L.Y. Lam, L.M. Cheung, K.F. Chania, X.S. Zhao, G.Q. Lu, Removal of heavy metal ions from wastewater by chemically modified plant wastes as adsorbents: a review, Catal. Today 68 (2001) 129–133.
[9] Z.F. Guo, R.X. Ma, G.J. Li, Degradation of phenol by nanomaterial TiO_2 in wastewater, Chem. Eng. J. 119 (2006) 55–59.
[10] S. Dutta, J.K. Basu, R.N. Ghar, Studies on adsorption of p-nitrophenol on charred saw-dust, Sep. Purif. Technol. 21 (2001) 227–235.
[11] B. Xing, W.B. McGill, M.J. Dudas, Mechanism of slow desorption of organic compounds from sediments: a study using model sorbents, Environ. Sci. Technol. 28 (1994) 466–473.
[12] F.A. Banat, B. Al-Bashir, S. Al-Asheh, O. Hayajneh, Adsorption of phenol by bentonite, Environ. Pollut. 101 (2000) 391–398.
[13] Y. Kikuchi, Q. Qian, M. Machida, H. Tatsumoto, Effect of ZnO loading to activated carbon on Pb(II) adsorption from aqueous solution, Carbon 44 (2006) 195–202.
[14] B.C. Pan, X. Zhang, W.M. Zhang, J.Z. Zheng, B.J. Pan, J.L. Chen, Q.X. Zhang, Adsorption of phenolic compounds from aqueous solution onto a macroporous polymer and its aminated derivative: isotherm analysis, J. Hazard. Mater. 121 (2005) 233–324.
[15] M. Ma, D. Li, New organic nanoporous polymers and their inclusion complexes, Chem. Mater. 11 (1999) 872–874.
[16] C.T. Kresge, M.E. Leonowicz, W.J. Roth, J.C. Vartuli, J.S. Beck, Ordered mesoporous molecular sieves synthesized by a liquid–crystal template mechanism, Nature 359 (1992) 710–712.
[17] M. Anbia, M. Lashgari, Synthesis of amino-modified ordered mesoporous silica as a new nano sorbent for the removal of chlorophenols from aqueous media, Chem. Eng. J. 150 (2009) 555–560.
[18] M. Anbia, N. Mohammadi, A nanoporous adsorbent for removal of furfural from aqueous solutions, Desalination 249 (2009) 150–153.
[19] M. Anbia, N. Mohammadi, K. Mohammadi, Fast and efficient mesoporous adsorbents for the separation of toxic compounds from aqueous media, J. Hazard. Mater. 176 (2010) 965–972.
[20] R. Ryoo, S.H. Joo, S. Jun, Synthesis of highly ordered carbon molecular sieves via template-mediated structural transformation, J. Phys. Chem. B 103 (1999) 7743–7746.
[21] R. Ryoo, S.H. Joo, S. Jun, T. Tsubakiyama, O. Terasaki, Ordered mesoporous carbon molecular sieves by templated synthesis by templated synthesis: the structural varieties, Stud. Surf. Sci. Catal. 135 (2001) 150–157.
[22] S. Jun, S.H. Joo, R. Ryoo, M. Kruk, M. Jaroniec, Z. Liu, T. Ohsuna, O. Terasaki, Synthesis of new, nanoporous carbon with hexagonally ordered mesostructure, J. Am. Chem. Soc. 122 (2000) 10712–10713.
[23] M. Kaneda, T. Tsubakiyama, A. Carlsson, Y. Sakamoto, T. Ohsuna, O. Terasaki, S.H. Joo, R. Ryoo, Structural study of mesoporous MCM-48 and carbon networks synthesized in the spaces of MCM-48 by electron crystallography, J. Phys. Chem. B 106 (2002) 1256–1266.
[24] S.H. Joo, S.J. Choi, I. Oh, J. Kwak, Z. Liu, O. Terasaki, R. Ryoo, Ordered nanoporous arrays of carbon supporting high dispersions of platinum nanoparticles, Nature 412 (2001) 169–172.
[25] W. Guo, F. Su, X.S. Zhao, Ordered mesostructured carbon templated by SBA-16 silica, Letters to the Editor, Carbon 43 (2005) 2423–2426.
[26] M. Anbia, A. Ghaffari, Adsorption of phenolic compounds from aqueous solutions using carbon nanoporous adsorbent coated with polymer, Appl. Surf. Sci. 255 (2009) 9487–9492.
[27] M. Anbia, S.E. Moradi, Removal of naphthalene from petrochemical wastewater streams using carbon nanoporous adsorbent, Appl. Surf. Sci. 255 (2009) 5041–5047.
[28] G. Taguchi, Introduction to Quality Engineering, McGraw-Hill, New York, USA, 1990.
[29] K.T. Chiang, Optimization of the design parameters of Parallel-Plain Fin heat sink module cooling phenomenon based on the Taguchi method, Int. Commun. Heat Mass Transfer 32 (2005) 1193–1201.
[30] T.Y. Wang, C.Y. Huang, Improving forecasting performance by employing the Taguchi method, Eur. J. Oper. Res. 176 (2007) 1052–1065.
[31] C.S. Chou, R.Y. Yang, J.H. Chen, S.W. Chou, The optimum conditions for preparing the lead-free piezoelectric ceramic of $Bi_{0.5}Na_{0.5}TiO_3$ using the Taguchi method, Powder Technol. 199 (2010) 264–271.
[32] M. Sadrzadeh, T. Mohammadi, Seawater desalination using electrodialysis, Desalination 221 (2008) 440–447.
[33] H. Atil, Y. Unver, A different of experimental design: Taguchi method, Biol. Sci. 3 (2000) 1538–1540.
[34] M. Colilla, F. Balas, M. Manzano, M. Vallet-Regi, Novel method to synthesize ordered mesoporous silica with high surface areas, Solid State Sci. 10 (2008) 408–415.
[35] P.A. Bazuła, A.H. Lu, J.J. Nitz, F. Schuth, Surface and pore structure modification of ordered mesoporous carbons via a chemical oxidation approach, Micropor. Mesopor. Mater. 108 (2008) 266–275.
[36] E. Ayranci, N. Hoda, Adsorption kinetics and isotherms of pesticides onto activated carbon-cloth, Chemosphere 60 (2005) 1600–1607.
[37] G. Purna Chandra Rao, S. Satyaveni, A. Ramesh, K. Seshaiah, K.S.N. Murthy, N.V. Choudary, Sorption of cadmium and zinc from aqueous solutions by zeolite 4A, zeolite 13X and bentonite, J. Environ. Manage. 81 (2006) 265–272.
[38] G. Mckay, H.S. Blair, J.R. Gardener, Adsorption of dyes on chitin. I. Equilibrium studies, J. Appl. Polym. Sci. 27 (1982) 3043–3057.
[39] A. Seco, P. Marzal, C. Gabaldo, Adsorption of Heavy metals from aqueous solutions onto activated carbon in single Cu and Ni systems and in binary Cu.Ni, Cu.Cd and Cu.Z systems, J. Chem. Technol. Biotechnol. 68 (1997) 23–30.
[40] R. Leyva-Ramos, L. Fuentes-Rubio, R.M. Guerrero-Coronado, J. Mendoza-Barron, Adsorption of trivalent chromium from aqueous solutions onto activated carbon, J. Chem. Technol. Biotechnol. 62 (1995) 64–67.
[41] P. Marzal, A. Seco, C. Gabaldo, J. Ferrer, Cadmium and zinc adsorption onto activated carbon: influence of temperature, pH and metal/carbon ratio, J. Chem. Technol. Biotechnol. 66 (1996) 279–285.
[42] S.G. Wang, W.X. Gong, X.W. Liu, Y.W. Yao, B.Y. Gao, Q.Y. Yue, Removal of lead(II) from aqueous solution by adsorption onto manganese oxide-coated carbon nanotubes, Sep. Purif. Technol. 58 (2007) 17–23.
[43] H. Tamura, R. Furuichi, Adsorption affinity of divalent heavy metal ions for metal oxides evaluated by modeling with the Frumkin isotherm, J. Colloid Interface Sci. 195 (1997) 241–249.
[44] K. Kadirvelu, C. Jyotsna Goel, Rajagopal Sorption of lead, mercury and cadmium ions in multi-component system using carbon aerogel as adsorbent, J. Hazard. Mater. 153 (2008) 502–507.